

We are IntechOpen, the world's leading publisher of Open Access books Built by scientists, for scientists

6,900

Open access books available

186,000

International authors and editors

200M

Downloads

Our authors are among the

154

Countries delivered to

TOP 1%

most cited scientists

12.2%

Contributors from top 500 universities



WEB OF SCIENCE™

Selection of our books indexed in the Book Citation Index
in Web of Science™ Core Collection (BKCI)

Interested in publishing with us?
Contact book.department@intechopen.com

Numbers displayed above are based on latest data collected.
For more information visit www.intechopen.com



Quantification of Laser Polarization by Position Dependent Refractive Indices

Yong Woon Parc and In Soo Ko
*Department of Physics, Pohang University
of Science and Technology, Pohang
Korea*

1. Introduction

The electro-optic (EO) crystals used in the generation of tera-hertz radiation [Shan et al, 2000; Wen & Lindenberg, 2009; Shen et al., 2008] can be applied to non-invasive measurements of the electron bunch in the accelerator. The bunch length and arrival time of the electron bunch with respect to the laser can be measured with this technique. The electric field generated by the electron bunch changes the optical properties of the EO crystal. The laser passing through the EO crystal will thus experience a modulation in the polarization state. The amount of optical power modulation, which can be detected by detectors such as photodiodes and cameras, can be calculated by Jones's matrices [Jones, 1941; Hecht, 2002].

In recent years, the EO technique has been implemented to measure femtosecond electron bunches with high energy at several facilities such as the free-electron laser for infrared experiments (FELIX), the sub-picosecond pulse source (SPPS), and the free-electron laser in Hamburg (FLASH) [Yan et al, 2000; Wilke et al., 2002; Berden et al., 2004; Cavalieri et al., 2005; Casalbuoni et al., 2008; Steffen et al., 2009]. In these applications, the electric field from the electron bunch makes a finite angle with the crystallographic axis, because the electric field is generated radially from the electron bunch.

In a real diagnostics setup, the principal axes at the passing position of the laser in the EO crystal are no longer 45° with respect to the crystallographic axes. However, the polarization vector of the laser is usually fixed as parallel to a crystallographic axis of the EO crystal in the measurement. When an electric field is applied to the EO crystal, it shows a birefringence which is described by an ellipsoid equation of refractive indices. If the ellipsoid equation can be expressed without any cross term between the three axes in a coordinate system, they are called the principal axes. If a linearly polarized laser is passing through the EO crystal with an external electric field applied to it, the polarization of the laser is modulated elliptically or even circularly. Conventional theories to describe the measurement result of an electron bunch with EO crystal have only used the principal axes and the principal refractive indices. To quantify the polarization state, we need to define amplitudes and phases of the electric field components of the laser. If the amplitudes of the decomposed electric field are the same, we need the phase information only to quantify the polarization state. To decompose the electric field with the same amplitude, we need to choose decomposition axes at 45° with respect to the polarization vector. The spatial

decoding method uses a laser propagated to the EO crystal at a certain angle with respect to the surface of the crystal to measure the electron bunch [Cavaliere et al., 2005; Parc et al., 2009a]. In this situation, we need to know refractive indices in the plane perpendicular to the propagation direction.

The principal axes are not in the plane in the spatial decoding method. Thus, the principal axes are not a good choice for the decomposition of the polarization vector. Even though this problem exists in the application of the EO technique to the accelerator, simulations for the EO measurement of the electron bunch have been conducted without consideration of this problem [Casalbuoni et al., 2008]. Refractive indices along the 45° axes with respect to the polarization vector are introduced by the authors in Ref. [Parc et al., 2009a] to compare a measurement result with the electron bunch and the simulation result.

This article presents the detailed derivation process of the refractive indices along the 45° axes with respect to the polarization vector in the plane perpendicular to the laser propagation direction. The optical power modulation of the laser is calculated by the matrix multiplication method invented by Jones with newly derived refractive indices. These refractive indices can be used to directly express experimental and numerical study results of the polarization state in the laser by the relative phase shift. The variation of the relative phase shifts will be presented when the distance between the electron bunch and EO crystal are changed. The paper is organized as follow: The theory of EO effect is reviewed in Section 2. The theory of detection of the optical power modulation of the laser is developed in Section 3. An experiment conducted in FLASH is analyzed in Section 4. Simulation results are shown in Section 5, and the conclusion and discussion are provided in Section 6.

2. Theory of refractive indices in electro-optic crystal

There are two methods to get the principal refractive indices. The two methods are reviewed in next two subsections, respectively. The principal refractive indices calculated by the two methods are revealed as the same and new form of the principal refractive indices is also obtained in this review.

2.1 Principal refractive indices obtained by solving the eigenvalue equation

In this subsection, the method introduced in Ref. [Casalbuoni et al., 2008] is reviewed to compare the principal refractive indices calculated in the reference with the other results which will be introduced in next subsection. The refractive indices of EO crystal such as GaP are obtained from an ellipsoid equation [Yariv & Yeh, 2003], written as,

$$\frac{1}{n_0^2}(x^2 + y^2 + z^2) + 2r_{41}(E_x yz + E_y zy + E_z xy) = 1 \quad (1)$$

where n_0 is the initial refractive index, r_{41} is the electro-optic constant, and E_i ($i = x, y, z$) is the electric field component applied to the crystal along the corresponding axis as shown in Fig. 1(a). If the ellipsoid equation can be expressed without any cross term in a certain coordinate system, the coordinates are called the principal axes. The X, Y, Z axes in Fig. 1(b) are defined as the crystallographic axes of the EO crystal in this study.

The optical property of isotropic EO crystal depends on the direction of the applied electric field [Berden et al., 2004; Parc et al., 2009a]. Thus, the directions of the principal axes of the isotropic crystal are changed along the direction of applied electric field. A correlation

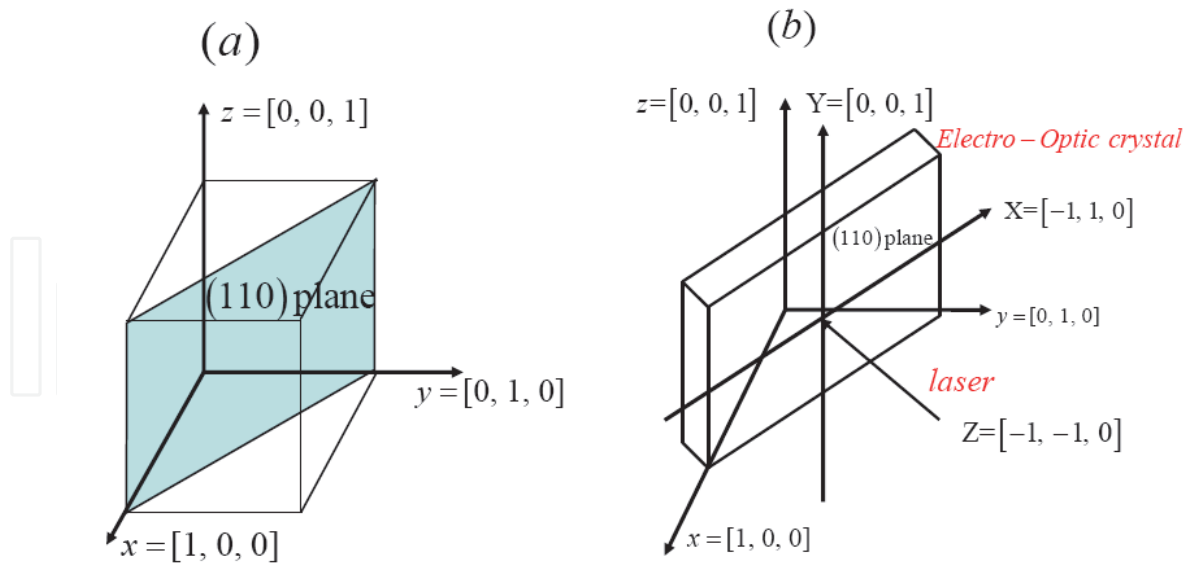


Fig. 1. (a) Right angle coordinate system of the crystal axis and (110) plane. The electro-optic crystal is cut in (110) plane. (b) The coordinate system X, Y, Z is shown with the electro-optic crystal. Laser will be passing into the Z direction in the experiment.

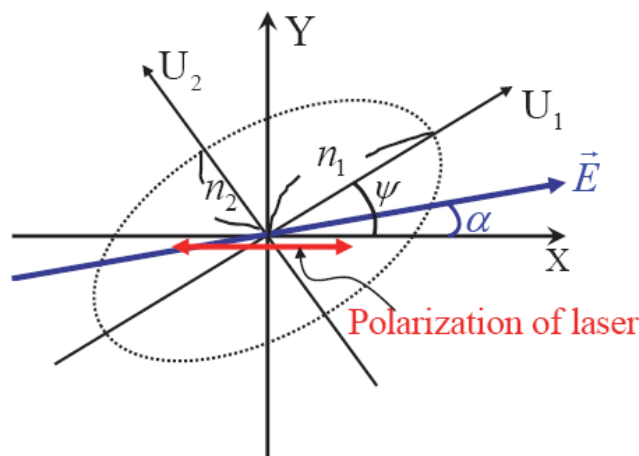


Fig. 2. The index ellipse is shown with the principal axis U_1 and U_2 . α represents the angle between the crystal axis X and the applied electric field E . The ψ is the angle between the principal axis and the crystal axis. The probe laser is linearly polarized as parallel to the X axis.

between the direction of the principal axes and the external applied electric field can be calculated from the constant energy surface in the electric displacement vector space and the impermeable tensor that is linear to the electric field [Yariv & Yeh, 2003; Casalbuoni et al. 2008]. The electric field vector from the electron beam with an angle α with respect to $X = [-1, 1, 0]$ axis in Fig. 2 can be represented as

$$\vec{E} = E \cdot \begin{pmatrix} -\cos \alpha / \sqrt{2} \\ \cos \alpha / \sqrt{2} \\ \sin \alpha \end{pmatrix} = \begin{pmatrix} E_x \\ E_y \\ E_z \end{pmatrix} \tag{2}$$

in the (x, y, z) coordinate system, where E is the amplitude of the electric field. The impermeability tensor in the (x, y, z) coordinate system with the same electric field vector is defined as

$$\eta = \frac{1}{n_0^2} \begin{pmatrix} 1 & 0 & 0 \\ 0 & 1 & 0 \\ 0 & 0 & 1 \end{pmatrix} + r_{41} \cdot E \cdot \begin{pmatrix} 0 & \sin \alpha & \cos \alpha / \sqrt{2} \\ \sin \alpha & 0 & -\cos \alpha / \sqrt{2} \\ \cos \alpha / \sqrt{2} & -\cos \alpha / \sqrt{2} & 0 \end{pmatrix}. \quad (3)$$

The eigenvalue equation is given by

$$\eta X = \xi X \quad \text{or} \quad |\eta - \xi I| = 0. \quad (4)$$

Principal axes of the refractive index ellipsoid equation and the eigenvalues can be known by solving Eq. (4) with the impermeability tensor. The eigenvalues of the impermeability tensor are, then,

$$\begin{aligned} \xi_1 &= \frac{1}{n_0^2} - \frac{r_{41}E}{2} \left(\sin \alpha + \sqrt{1 + 3 \cos^2 \alpha} \right), \\ \xi_2 &= \frac{1}{n_0^2} - \frac{r_{41}E}{2} \left(\sin \alpha - \sqrt{1 + 3 \cos^2 \alpha} \right), \\ \xi_3 &= \frac{1}{n_0^2} + r_{41}E \sin \alpha. \end{aligned} \quad (5)$$

The eigenvectors U_1, U_2 can be obtained as shown in Fig. 2. The refractive index ellipsoid equation in Eq. (1) is now transformed into the form

$$\frac{U_1^2}{\xi_1^{-1}} + \frac{U_2^2}{\xi_2^{-1}} + \frac{U_3^2}{\xi_3^{-1}} = 1 \quad \text{or} \quad \frac{U_1^2}{n_1^2} + \frac{U_2^2}{n_2^2} + \frac{U_3^2}{n_3^2} = 1. \quad (6)$$

The principal refractive indices n_i can, then, be following:

$$n_i^2 = \xi_i^{-1}. \quad (7)$$

If the following relation is available in Eq. (5)

$$r_{41}E \ll 1/n_0^2, \quad (8)$$

the indices of refraction of the crystal along the principal axes in Fig. 2 are given as [Casalbuoni et al. 2008],

$$\begin{aligned} n_1 &= n_0 + \frac{n_0^3 r_{41} E}{4} \left(\sin \alpha + \sqrt{1 + 3 \cos^2 \alpha} \right), \\ n_2 &= n_0 + \frac{n_0^3 r_{41} E}{4} \left(\sin \alpha - \sqrt{1 + 3 \cos^2 \alpha} \right), \\ n_3 &= n_0 - \frac{n_0^3 r_{41} E}{2} \sin \alpha \end{aligned} \quad (9)$$

where n_0 is the initial refractive index, r_{41} is the electro-optic constant, E is the electric field applied to the crystal, and a is the angle between the crystal axis and the electric-field. The relation of the angle ψ between the principal axis and the X axis and the angle a between the electric field and the X axis is given by [Casalbuoni et al. 2008; Parc et al., 2008a]

$$\cos 2\psi = \frac{\sin \alpha}{\sqrt{1 + 3 \cos^2 \alpha}} \quad (10)$$

2.2 Principal refractive indices obtained by coordinate transformation

In Ref. [Planken et al., 2001], another method is introduced to get the principal axes and the principal refractive indices. By transformation of the axes, the principal axes and the principal refractive indices can be obtained. The first transformation of the crystallographic axes x, y, z to new axes X, Y, Z in Fig. 1(b) is a rotation of 45° around the z axis,

$$\begin{aligned} x &= \frac{1}{\sqrt{2}}Z - \frac{1}{\sqrt{2}}X, \\ y &= \frac{1}{\sqrt{2}}Z + \frac{1}{\sqrt{2}}X, \\ z &= Y. \end{aligned} \quad (11)$$

The ellipsoid equation of Eq. (1) is now transformed into the new form in the new coordinated system X, Y, Z as

$$X^2 \left(\frac{1}{n_o^2} - E_z r_{41} \right) + \frac{Y^2}{n_o^2} + 2\sqrt{2}E_x r_{41}XY + Z^2 \left(\frac{1}{n_o^2} + E_z r_{41} \right) = 1. \quad (12)$$

To eliminate the remaining cross term between X and Y , we need one more rotation around Z axis as follow:

$$\begin{aligned} X &= U_1 \cos \psi - U_2 \sin \psi, \\ Y &= U_1 \sin \psi + U_2 \cos \psi, \\ Z &= U_3. \end{aligned} \quad (13)$$

Using the rotation relation Eq. (13), Eq. (12) is now expressed as

$$\begin{aligned} &U_3^2 \left(\frac{1}{n_o^2} + E_z r_{41} \right) + U_1^2 \left(\cos^2 \psi \left(\frac{1}{n_o^2} - E_z r_{41} \right) + \frac{1}{n_o^2} \sin^2 \psi + 2\sqrt{2}E_x r_{41} \cos \psi \sin \psi \right) \\ &+ U_2^2 \left(\sin^2 \psi \left(\frac{1}{n_o^2} - E_z r_{41} \right) + \frac{1}{n_o^2} \cos^2 \psi - 2\sqrt{2}E_x r_{41} \sin \psi \cos \psi \right) \\ &+ U_1 U_2 \left(-2 \cos \psi \sin \psi \left(\frac{1}{n_o^2} - E_z r_{41} \right) + \frac{(2 \sin \psi \cos \psi)}{n_o^2} + 2\sqrt{2}E_x r_{41} (-\sin^2 \psi + \cos^2 \psi) \right) = 1. \end{aligned} \quad (14)$$

There is a cross term between U_1 and U_2 . If the cross term is eliminated, we can get the principal axes and the principal refractive indices. Thus, the condition is

$$-2 \cos \psi \sin \psi \left(\frac{1}{n_o^2} - E_z r_{41} \right) + \frac{(2 \sin \psi \cos \psi)}{n_o^2} + 2\sqrt{2}E_x r_{41} (-\sin^2 \psi + \cos^2 \psi) = 0. \quad (15)$$

Using Eq. (2), Eq. (15) gives us next relation:

$$\tan 2\psi \tan \alpha = 2. \quad (16)$$

It is easy to show that Eq. (16) is a different expression of Eq. (10). Using Eq. (2) and after an algebra, Eq. (14) is now shown as more compact form

$$\begin{aligned} & U_3^2 \left(\frac{1}{n_o^2} + Er_{41} \sin \alpha \right) + U_1^2 \left(\frac{1}{n_o^2} - Er_{41} (\sin \alpha \cos^2 \psi + \cos \alpha \sin 2\psi) \right) \\ & + U_2^2 \left(\frac{1}{n_o^2} - Er_{41} (\sin \alpha \sin^2 \psi - \cos \alpha \sin 2\psi) \right) = 1. \end{aligned} \quad (17)$$

The principal refractive indices are now obtained with the same condition in Eq. (8),

$$\begin{aligned} n_1 &= n_0 + \frac{1}{2} n_0^3 r_{41} E (\sin \alpha \cos^2 \psi + \cos \alpha \sin 2\psi), \\ &= n_0 + \frac{1}{4} n_0^3 r_{41} E (\sin \alpha + \sqrt{1 + 3 \cos^2 \alpha}), \\ &= n_0 + \frac{1}{2} n_0^3 r_{41} E (\sin \alpha \sin^2 \psi + \sin(\alpha + 2\psi)). \end{aligned} \quad (18)$$

$$\begin{aligned} n_2 &= n_0 + \frac{1}{2} n_0^3 r_{41} E (\sin \alpha \sin^2 \psi - \cos \alpha \sin 2\psi), \\ &= n_0 + \frac{1}{4} n_0^3 r_{41} E (\sin \alpha - \sqrt{1 + 3 \cos^2 \alpha}), \\ &= n_0 + \frac{1}{2} n_0^3 r_{41} E (\sin \alpha \cos^2 \psi - \sin(\alpha + 2\psi)). \end{aligned} \quad (19)$$

The first expressions of n_1 and n_2 are the newly derived form in this review. The second expressions of n_1 and n_2 are derived in section A. The third expressions are shown to compare our results with Eq. (7) in Ref. [15Planken]. The second and the third expressions in n_1 and n_2 can be obtained also from the first expression by using the relation Eq. (16). Note that the angle definition a of the electric field in this review is equivalent with $a+90^\circ$ in Ref. [Planken et al., 2001]. The ψ in this study is expressed as θ in Ref. [Planken et al., 2001].

2.3 Refractive indices in the plane perpendicular to the laser propagation direction

The configuration for the measurement of the electron beam with EO crystal is shown in Fig. 3. A method called the spatial decoding is used to measure the bunch length and the timing jitter of the electron beam as shown in Fig. 3 [Cavalieri et al., 2005; Azima et al., 2006]. In the spatial decoding method, the laser pulse is propagated through the EO crystal with the incident angle φ_0 , and the timing information of the electron beam is converted to the spatial information of the image measured by an ICCD camera as shown in Fig. 3 [Cavalieri et al., 2005; Azima et al., 2006]. The modulation of the polarization of the laser can be measured by a prism. The prism in Fig. 3 splits the laser as horizontal and vertical components.

When an electron beam is propagating beside the EO crystal, the detail configuration around EO crystal is shown in Fig. 4(a). The red line in Fig. 4(a) represents the laser which

is shaped like a thin pencil. The principal axes U_1 , U_2 of the crystal is also shown in Fig. 4(a). The U_1 , U_2 , X , and Y axes are all in the same plane (110) which is described in Fig. 2. The front view of Fig. 4(a) is shown in Fig. 4(b). The angle between the crystallographic axis X and the electric field E from the electron beam is represented by a in Fig. 4(b). The y axis in Fig. 4(b) is the trace of the laser on the EO crystal. R is the distance between the electron beam and the laser passing position when the electron beam is arrived at the EO crystal. The perpendicular distance from the electron beam and the y axis is denoted by r_0 . The side view of Fig. 4(a) is drawn in Fig. 4(c). The pencil shape laser makes an incident angle φ_0 with EO crystal in the spatial decoding method [Cavalieri et al., 2005]. \vec{k} is the wave vector of the laser inside of EO crystal. The laser is propagating to the \vec{k} direction drawn as a dotted arrow. The angle φ_L is the angle between the laser and EO crystal inside of the crystal.

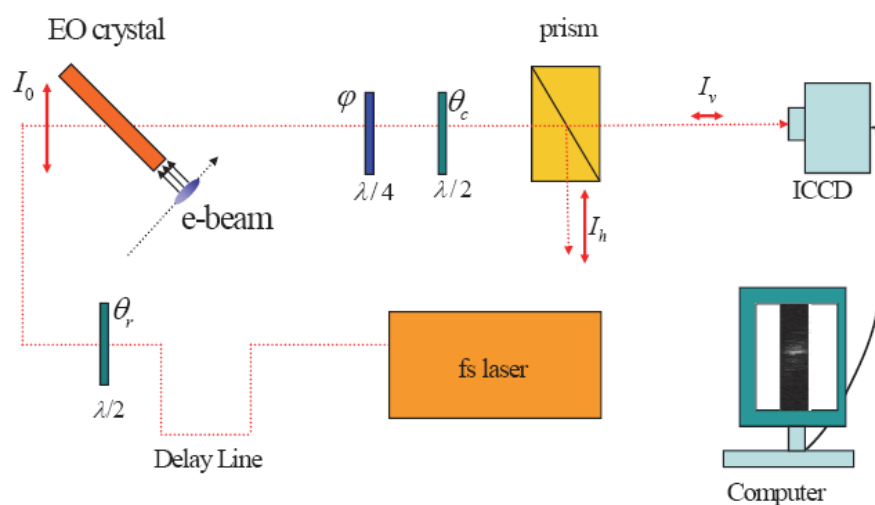


Fig. 3. Layout of the EO sampling experiment of electron beam in TEO setup at FLASH in DESY.

The linear polarization of the laser can be expressed as a vector which will be called as the polarization vector denoted as Ψ_L in Fig. 5(a). The inner parts of all axes in the ellipsoid are denoted by dotted lines in Fig. 5(a). \vec{k} is the wave vector of the laser shown in Fig. 4(c). A plane perpendicular to the wave vector \vec{k} will cut the ellipsoid, thus we can see an ellipse as shown in Fig. 5(a). The 45° axes with respect to the polarization vector are denoted by A and B in this study as shown in Fig. 5(a). A and B axes are in the same plane with the ellipse. Note that U_1 and U_2 axes are not in the same plane. The polarization vector Ψ_L can be also decomposed as two vectors denoted by Ψ_A and Ψ_B along the A and B axes, respectively, as shown in Fig. 5(a). The amplitude of the vector represents the electric field amplitude of the laser. In Fig. 5(a), Ψ_A is defined as a decomposed vector along A axis which makes 45° with the polarization vector Ψ_L of the laser. These vectors are all in the same plane. The ellipse and the A axis makes an intersection point M as shown in Fig. 5(a). The distance from the origin of the ellipsoid to the intersection point M will give new refractive index n_A along the A axis as shown in Fig. 5(b). Similarly, the refractive index along the B axis is denoted by n_B in Fig. 5(b).

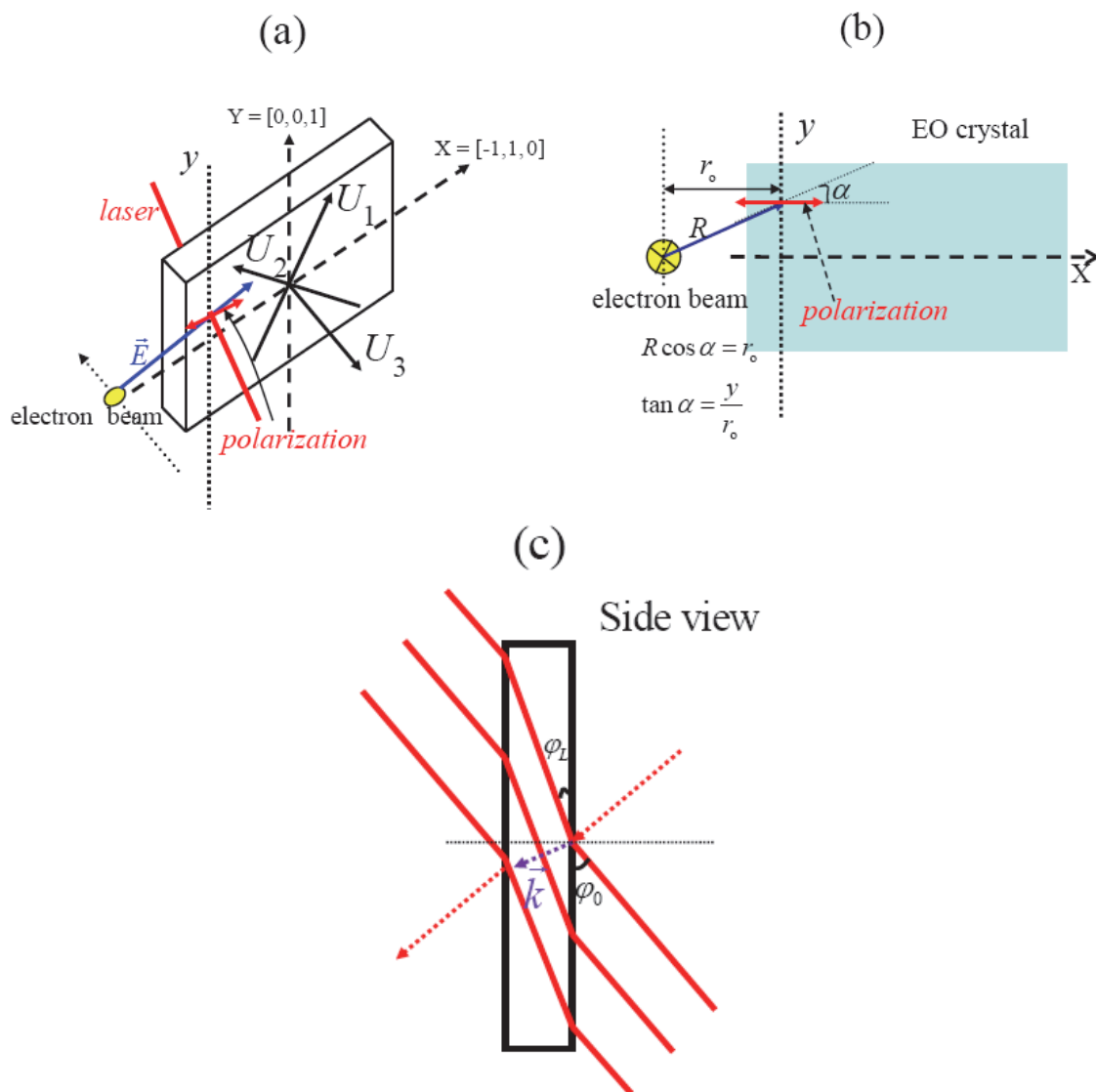


Fig. 4. Spatial decoding method in EO measurement of electron beam is shown with the principal axis

The angle of the prism in Fig. 3 determines the horizontal H and vertical V axis in Fig. 5(b). Because the polarization vector is usually fixed as parallel to X axis, we should control the prism angle such that the horizontal axis H to be matched with X axis as shown in Fig. 5(b). The polarization vector Ψ_L can be decomposed as two vectors denoted by Ψ_h and Ψ_v along the horizontal H and the vertical V axis, respectively. There is no vertical component of the polarization in Fig. 5(b). However, by the modulation of the polarization by passing through the EO crystal, the vertical component will be created and we can measure the vertical component by a prism as shown in Fig. 3. This is the key factor to measure the electron beam properties by EO crystal nondestructively. The G point in Fig. 5(b) is the projection point of the polarization vector Ψ_L to A axis.

The 3D configuration for the vector decomposition with the principal axes is shown in Fig. 6. The A axis in Fig. 5 is in the same direction with the OG line in Fig. 6. Note that OG line and X axis forms 45° angle as described in Fig. 5(b). For a given wave vector \vec{k} of the laser

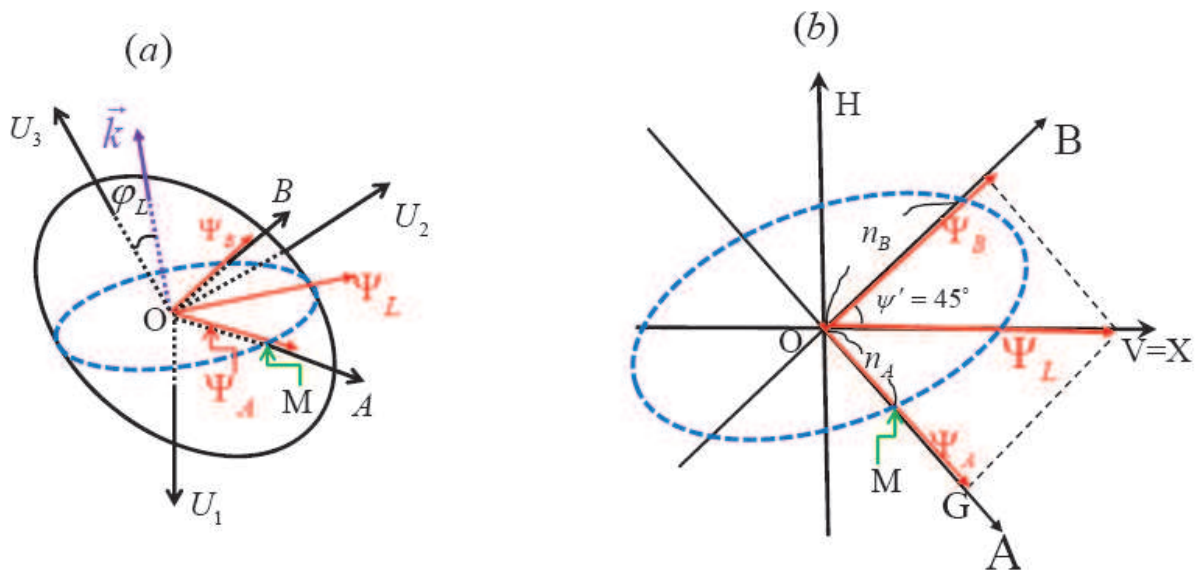


Fig. 5. (a) The index ellipsoid is shown with the principal axes $U_1, U_2,$ and U_3 . (b) The 2D configuration for the decomposition of the laser polarization vector Ψ_L . A and B axes make 45° with respect to the polarization vector Ψ_L . H and V axes are the horizontal and vertical axes in the AB plane. The polarization vector Ψ_L is fixed as parallel to the X axis. n_A and n_B are the refractive indices along A and B axes, respectively.

as shown in Fig. 5(a), the index n_A can be derived from the index ellipsoid equation and the OG line. The OG line will make an intersection point M with the ellipse as shown in Fig. 5(b). Our goal is to get an expression of the G point in the principal axes system to calculate the index n_A .

Lengths of OG, GF and FH in Fig. 6 are calculated as:

$$\begin{aligned}
 OG &= \Psi_L \cos(45^\circ) = \frac{1}{\sqrt{2}} \Psi_L = \Psi_A \\
 GF &= OG \sin(45^\circ) = \frac{1}{2} \Psi_L \\
 FH &= GF \cos(\varphi_L) = \frac{1}{2} \Psi_L \cos(\varphi_L)
 \end{aligned} \tag{20}$$

We need to know the G point in the principal axes U_1, U_2, U_3 system. Each component of the G point can be calculated as the projection of the OG line to each axis as shown:

$$\begin{aligned}
 GH &= GF \sin(\varphi_L) = \frac{1}{2} \Psi_L \sin(\varphi_L) = G_3 \\
 OH &= \sqrt{OF^2 + FH^2} = \frac{1}{2} \Psi_L \sqrt{1 + \cos^2 \varphi_L} \\
 OK &= OH \cos(\psi - \theta_L) = G_1 \\
 HK &= OH \sin(\psi - \theta_L) = -G_2
 \end{aligned} \tag{21}$$

The G point in the principal axes is now shown as:

$$\begin{aligned}
G &= (G_1, G_2, G_3) \\
&= (OK, -HK, GH) \\
&= \left(OH \cos(\psi - \theta_L), -OH \sin(\psi - \theta_L), \frac{1}{2} E_L \sin \varphi_L \right) \\
&= \frac{1}{2} \Psi_L \left(\cos(\psi - \theta_L) \sqrt{1 + \cos^2 \varphi_L}, -\sin(\psi - \theta_L) \sqrt{1 + \cos^2 \varphi_L}, \sin \varphi_L \right)
\end{aligned} \quad (22)$$

Next relation can be calculated easily from Eq. (22)

$$G_1^2 + G_2^2 + G_3^2 = \frac{1}{2}. \quad (23)$$

The projection line equations of the OG line to the planes generated by the principal axes U_1, U_2, U_3 are given by

$$\begin{aligned}
G_2 U_1 - G_1 U_2 &= 0 \\
G_3 U_2 - G_2 U_3 &= 0 \\
G_1 U_3 - G_3 U_1 &= 0
\end{aligned} \quad (24)$$

Using Eqs. (24) and (7), next relation can be derived

$$\left[\left(\frac{G_1}{n_1} \right)^2 + \left(\frac{G_2}{n_2} \right)^2 + \left(\frac{G_3}{n_3} \right)^2 \right] U_i^2 = G_i^2, \quad (25)$$

where i is the index for the principal axes U_1, U_2, U_3 . The refractive indices n_A for the A axis is derived by the distance from the origin of the ellipsoid to the intersection point M as shown in Fig. 5(a). Thus, the refractive index n_A along the A axis is defined as

$$n_A = \sqrt{U_1^2 + U_2^2 + U_3^2}. \quad (26)$$

The calculation of n_B for B axis is similar with n_A , not shown in this study. The two indices are [Parc et al., 2009a],

$$\begin{aligned}
n_A &= \sqrt{\frac{2}{\left(\frac{\sin^2(\psi - \theta_L)(1 + \cos^2 \varphi_L)}{n_1^2} \right) + \left(\frac{\cos^2(\psi - \theta_L)(1 + \cos^2 \varphi_L)}{n_2^2} \right) + \left(\frac{\sin^2 \varphi_L}{n_3^2} \right)}} \\
n_B &= \sqrt{\frac{2}{\left(\frac{\cos^2(\psi - \theta_L)(1 + \cos^2 \varphi_L)}{n_1^2} \right) + \left(\frac{\sin^2(\psi - \theta_L)(1 + \cos^2 \varphi_L)}{n_2^2} \right) + \left(\frac{\sin^2 \varphi_L}{n_3^2} \right)}}
\end{aligned} \quad (27)$$

We can also get the relation between the angle φ_L and θ_L .

$$\begin{aligned}
OF &= OH \cos(\theta_L) \\
(1 + \cos^2 \varphi_L) \cos^2 \theta_L &= 1
\end{aligned} \quad (28)$$

where φ_L is the angle between the wave vector \vec{k} and U_3 axis, θ_L is the angle between the line OH and X axis in Fig. 6(b). The refractive indices in Eq. (27) are converted into the principal refractive indices n_1 and n_2 if the angle φ_L is 0° and ψ is 45° . The formula of the relative phase shift Γ in this review is now given by

$$\Gamma = \frac{\omega_0 d}{c} (n_A - n_B). \quad (29)$$

where d is the crystal thickness, ω_0 is the center angular frequency of the laser pulse, and c is the speed of light.

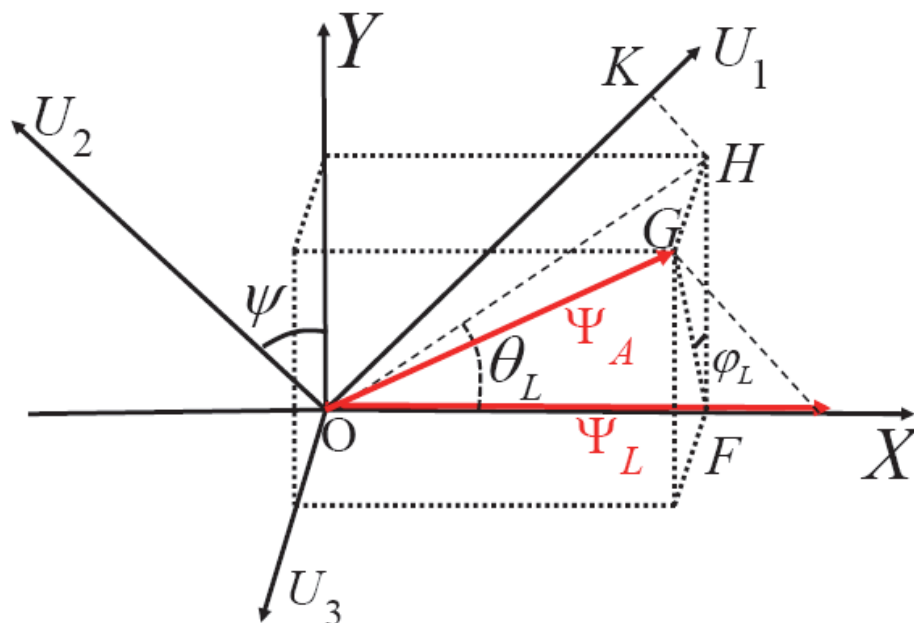


Fig. 6. The 3D configuration for the decomposition of the laser polarization vector Ψ_L . Ψ_A is the electric field component of the laser along the A axis. ψ is the angle between the principal axis and the crystal axis X. φ_L is the angle between the wave vector \vec{k} of the laser and the U_3 axis. θ_L is the angle between OH and X axis. The probe laser is linearly polarized as parallel to the X axis. ψ' is the angle between the A axis and the crystal axis X.

3. Theory for the detection of the modulation of the polarization

The polarization of the laser can be rotated by a half wave plate at the front of the EO crystal in a certain experimental situation as shown Fig. 3. This half wave plate will be named as 'Rotator' in this study. To increase the signal to noise ratio of the measurement result, a half wave plate and a quarter wave plate can be used in the downstream of the EO crystal [Steffen et al., 2009, Parc et al., 2008a]. The half wave plate in the downstream of EO crystal will be named as 'Compensator' in this study. In the next matrices and equations, Γ is the phase difference between the two decomposed vectors of the laser along A and B axes given by Eq. (29), θ_r is the angle of the rotator, θ_c is the angle of the compensator, φ is the angle of quarter wave plate, and ψ' is the angle between the A axis and X axis in the crystal as shown in Fig. 5(a). For the general purpose, the angle ψ' is set as arbitrary value in the

theory. To use the theory in the analysis of the experimental result, this angle is set to be 45° because the polarization vector is set as parallel with X axis as shown in Fig. 5(b). The rotation matrix R , Jones matrices for the half (H) wave plate, quarter (Q) wave plate, and EO crystal (EO) are given by, respectively,

$$\begin{aligned} \Gamma R &= \begin{pmatrix} \cos \zeta & -\sin \zeta \\ \sin \zeta & \cos \zeta \end{pmatrix} \\ EO(\Gamma) &= \begin{pmatrix} e^{-i\Gamma/2} & 0 \\ 0 & e^{i\Gamma/2} \end{pmatrix} \\ Q &= \begin{pmatrix} e^{-i\pi/4} & 0 \\ 0 & e^{i\pi/4} \end{pmatrix} \\ H &= \begin{pmatrix} e^{-i\pi/2} & 0 \\ 0 & e^{i\pi/2} \end{pmatrix} \end{aligned}$$

where ζ represents the angle of each wave plate with respect to the laser polarization direction in the measurement. The initial polarization vector in front of the rotator in Fig. 3 can be represented by 2×1 matrix such as

$$\Psi_L = \begin{pmatrix} 1 \\ 0 \end{pmatrix}.$$

All quantities of the laser such as the amplitude of the electric field and the intensity are normalized by its maximum value in all formulae for the convenience of derivation.

The horizontal electric field Ψ_h of the laser after passing through all optical components in Fig. 3 can be calculated by the product of matrices:

$$\Psi_h = \begin{pmatrix} 0 & 1 \end{pmatrix} \cdot R[-\theta_c] \cdot H \cdot R[\theta_c] \cdot R[-\varphi] \cdot Q \cdot R[\varphi] \cdot R[-\psi'] \cdot EO(\Gamma) \cdot R[\psi'] \cdot R[-\theta_r] \cdot H \cdot R[\theta_r] \cdot \begin{pmatrix} 1 \\ 0 \end{pmatrix}. \quad (30)$$

The intensity I_h of the horizontal component is proportional to the square of the horizontal electric field, and the normalized expression is given by:

$$\begin{aligned} I_h(\theta_c, \varphi, \psi', \theta_r; \Gamma) &= \Psi_h^2 \\ &= \frac{1}{2} \left[\begin{aligned} &\sin(\Gamma) \sin(4\theta_c - 2\varphi) \sin(4\theta_r - 2\psi') \\ &+ \left\{ \sin^2(2(\theta_c - \theta_r)) + \sin^2(2(\theta_c + \theta_r - \varphi)) \right\} \cos^2(\Gamma/2) \\ &+ \left\{ \sin^2(2(\theta_c + \theta_r - \psi')) + \sin^2(2(\theta_c - \theta_r - \varphi + \psi')) \right\} \sin^2(\Gamma/2) \end{aligned} \right]. \quad (31) \end{aligned}$$

The vertical electric field Ψ_v can be obtained by the similar calculation:

$$\Psi_v = \begin{pmatrix} 1 & 0 \end{pmatrix} \cdot R[-\theta_c] \cdot H \cdot R[\theta_c] \cdot R[-\varphi] \cdot Q \cdot R[\varphi] \cdot R[-\psi'] \cdot EO(\Gamma) \cdot R[\psi'] \cdot R[-\theta_r] \cdot H \cdot R[\theta_r] \cdot \begin{pmatrix} 1 \\ 0 \end{pmatrix}. \quad (32)$$

The intensity I_v of the vertical component is proportional to the square of the vertical electric field, and the normalized expression is also shown as:

$$\begin{aligned}
 I_v(\theta_c, \varphi, \psi', \theta_r : \Gamma) &= \Psi_v^2 \\
 &= \frac{1}{2} \left[\begin{aligned} &-\sin(\Gamma)\sin(4\theta_c - 2\varphi)\sin(4\theta_r - 2\psi') \\ &+ \left\{ \cos^2(2(\theta_c - \theta_r)) + \cos^2(2(\theta_c + \theta_r - \varphi)) \right\} \cos^2(\Gamma / 2) \\ &+ \left\{ \cos^2(2(\theta_c + \theta_r - \psi')) + \cos^2(2(\theta_c - \theta_r - \varphi + \psi')) \right\} \sin^2(\Gamma / 2) \end{aligned} \right]. \quad (33)
 \end{aligned}$$

The intensity of the horizontal part of the laser through the EO crystal and wave plates can be derived from Eq. (31). If we set the angle ψ' to be 45° as shown in Fig. 5(b) and the rotator angle θ_r is 0° , we can obtain the intensity function for the horizontal part of the laser and is given by [Steffen et al., 2009, Parc et al., 2008a]:

$$I_h(\theta_c, \varphi, \psi' = 45^\circ, \theta_r = 0^\circ : \Gamma) = [1 - \cos(\Gamma)\cos(4\theta_c - 2\varphi)\cos(2\varphi) - \sin(\Gamma)\sin(4\theta_c - 2\varphi)] / 2 \quad (34)$$

This kind of detection scheme is called as 'Near Crossed Polarizer' scheme [Steffen et al., 2009]. The angles of the quarter wave plate and compensator is usually set as a few degrees in the experiment [Parc et al., 2008a]. The intensity of the vertical part of the laser is also calculated as:

$$I_v(\theta_c, \varphi, \psi' = 45^\circ, \theta_r = 0^\circ : \Gamma) = [1 + \cos(\Gamma)\cos(4\theta_c - 2\varphi)\cos(2\varphi) + \sin(\Gamma)\sin(4\theta_c - 2\varphi)] / 2. \quad (35)$$

The difference between two components is easily calculated as

$$\Delta I \equiv I_v - I_h = \cos(\Gamma)\cos(4\theta_c - 2\varphi)\cos(2\varphi) + \sin(\Gamma)\sin(4\theta_c - 2\varphi) \quad (36)$$

For the balanced detection, the compensator angle θ_c should be set as 0° , the quarter wave plate angle φ should be set as 45° and the result is given by

$$\Delta I \equiv I_v - I_h = \sin(\Gamma). \quad (37)$$

This is well known formula derived with principal refractive indices [Casalbuoni et al., 2008]. Note that the relative phase Γ in Eq. (37) is defined by Eq. (29) with refractive indices given by Eq. (27).

4. Experiment

A test experiment was conducted to see the peak change in the CCD image with the change of laser arrival time with respect to the electron bunch at FLASH facility in DESY with the configuration in Fig. 3. The GaP crystal in this experiment was $180 \mu\text{m}$ thick. The radial distances between the electron bunch and the crystal were 3, 2.5 and 2 mm. The total charge Q of the electron bunch in the measurement was 0.6 nC and the beam energy was 682 MeV. Arrival timing jitter of the electron bunch can be measured with an EO crystal due to the change of the crossing position of the laser as the electron bunch arrives [Cavalieri et al., 2005]. The arrival timing information can be extracted from the spatial information of the laser intensity measured by ICCD camera. When the arrival timing of electron bunch with respect to the laser is changed, the modulation of polarization of the laser will also be changed. To investigate the modulation, the laser delay was controlled with a certain delay

time with respect to the electron beam and the vertical component of the laser was measured by ICCD camera. Changing the laser arrival time control the crossing positions of the laser with the EO crystal when the electron beam arrived at the EO crystal. The movement of the signal peak in the ICCD image was observed due to the change of crossing position of the laser as the electron bunch arrives at the EO crystal.

The plots in Figure 7 indicate the arrival time of the electron bunch with respect to the laser beam as observed by the ICCD camera. The time axis can be converted to the transverse length of the laser pulse [Azima et al., 2006]. A background measurement without an electron bunch is shown in Fig. 7 (a). A measurement result with the electron bunch is shown in Fig. 7(b). The background is subtracted from the result in Fig. 7(c). It shows a clear signal peak around 9 ps. Several measurement results with different arrival times of the laser are overlapped in Fig. 7(d). The peaks are moving by controlling of the laser arrival time, and the peak heights are also changed.

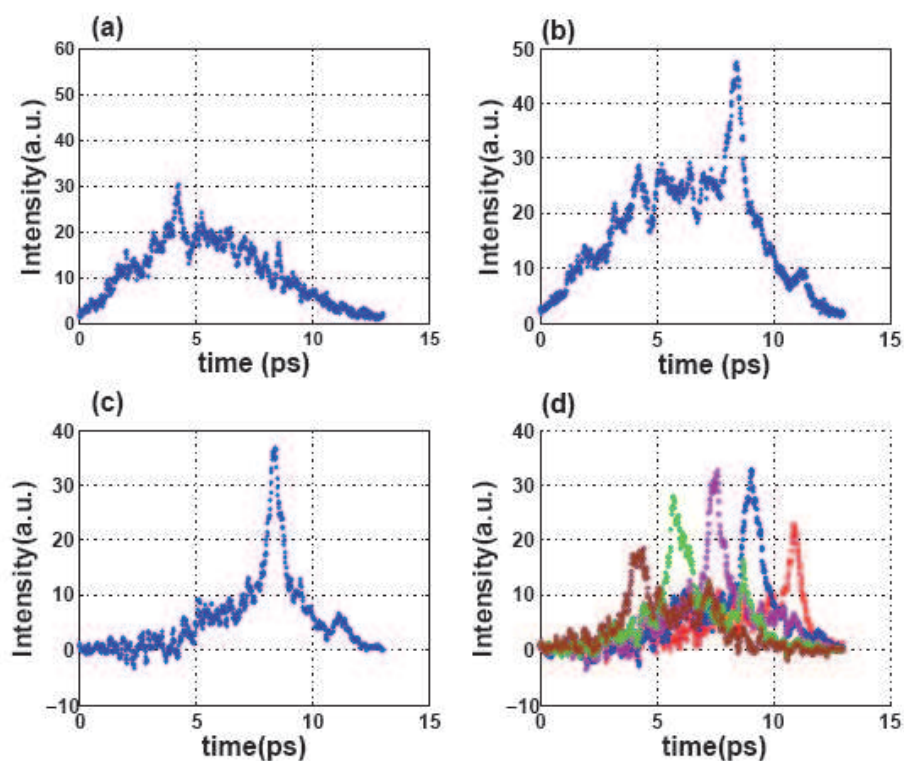


Fig. 7. Electron beam measurement by TEO setup at FLASH. The GaP crystal thickness is 180 μm . The distance between the electron beam and the laser at the crystal is 3 mm on average. The half wave plate angle is 0° and the quarter wave plate angle is -2° . X-axis represent the arrival time of the electron beam with respect to the laser beam. (a) The background measurement without electron beam. (b) The measurement result of the electron beam. (c) The difference between (a) and (b) is shown in (c). (d) Several measurement results with the change of the laser arrival time.

The measurement result must be expressed in terms of the relative phase shift Γ in Eq. (29) by using refractive indices in Eq. (27) to compare it with the simulation result. The measurement result can be analyzed in terms of the relative phase shift Γ with Jones matrices of the each wave plates as mentioned in Section 3 [Parc et al., 2008a, 2009b]. The analysis of the measured data in terms of the relative phase shift in Eq. (29) is shown in Fig.

8. The y axis in Fig. 8 represents the same axis shown in Fig. 4. The origin of the y axis is determined as the place where the relative phase shift reaches its maximum. Measurements are done with three r_o values defined in Fig. 4(b). The dots are the result with $r_o = 3$ mm, the squares are with $r_o = 2.5$ mm, and the triangles are with $r_o = 2$ mm. The relative phase shifts with the same condition of the electron beam show rapid change in spite of small changes of y as shown in Fig. 8. The smallest r_o has a higher relative phase shift at $y = 0$ mm. The peak value in Fig. 8 is about 12° . We define the degree of polarization as 0% for the linear polarization and 100% for the circular polarization. In our experimental result, we can conclude that the laser is 13% elliptically polarized by the electron beam with respect to the linear polarization.

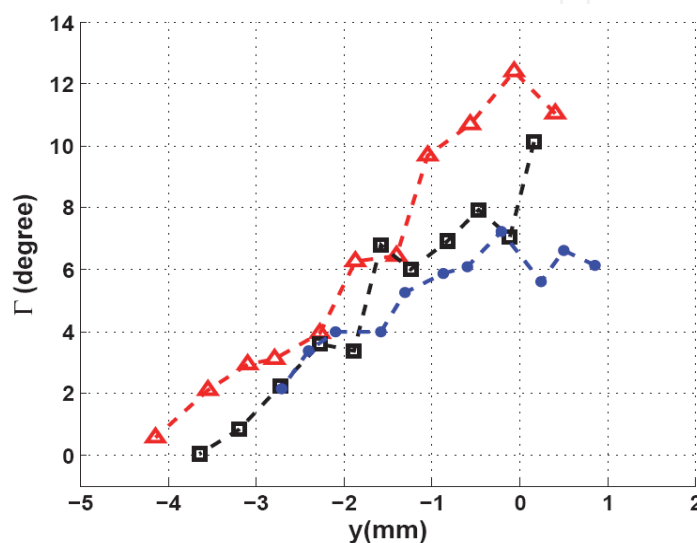


Fig. 8. The analysis results of the experiment in Fig. 6 in terms of the relative phase shift with new refractive indices for different distance r_o at $y = 0$ mm ($a = 0^\circ$) case are shown. The dots are the result with $r_o = 2$ mm, the squares are with $r_o = 2.5$ mm, and the triangles are with $r_o = 3$ mm. y is the laser passing position in the crystal along the angle a in Fig. 4. The total beam charge Q measured in the experiment is 0.6 nC.

5. Simulation

The measurement of an electron bunch with a EO crystal is also simulated. The GaP crystal has a frequency dependent refractive index [Casalbuoni et al., 2008]. The electric field profile from the electron bunch is expanded to a Fourier series to know the response of the Fourier component inside the crystal [Parc et al., 2007, 2008b]. Each Fourier component propagates at a different speed according to the real part of the complex refractive index [Casalbuoni et al., 2008]. The speed difference between the two decomposed vectors of the laser polarization makes the polarization modulation of the laser.

The simulation carefully considered the important aspects of the propagation of the electric field in the EO crystal [Parc et al., 2008b, 2009a,]. The electric field affecting the laser is not constant owing to the difference of the group velocity between the laser and the electric field. In this simulation, the crystal was divided into N sections to calculate the total relative phase shift of the laser during its propagation. The total relative phase shift with new refractive indices is the sum of each relative phase shift at each section as shown by

$$\Gamma = \sum_{j=1}^N \frac{d}{\lambda N} (n_A(E_j) - n_B(E_j)), \quad (38)$$

where all the parameters are same as those of Eq. (14) except that the index j is used to denote the j th section of the crystal, and N is the number of sections to be summed. The thickness of GaP was 180 μm , which is the same as the experiment. The electron bunch was assumed to have a Gaussian distribution. The beam charge q for the electron beam was 0.1 nC. The electron beam charge in the experiment is larger than the charge used in the simulation because the shape of the electron beam was not Gaussian [Parc et al., 2009b]. The configuration in the simulation is the same as in the experiment.

A simulated signal output with the electron bunch expressed by the relative phase shift Γ is shown in Fig. 9. In this figure, τ is the time delay between the probing laser pulse and the electric field at the surface of EO crystal in the simulation [Casalbuoni et al., 2008]. Peak values of the phase shift Γ in Fig. 9 for different distances r_0 along the y axis are presented in Fig. 10. The range of y axis is determined as the same with Fig. 8. The r_0 values were the same as in Fig. 8. The dots are the results with $r_0 = 3$ mm, the squares with $r_0 = 2.5$ mm, and the triangles with $r_0 = 2$ mm. These results are similar to the experimental results in Fig. 8. The relative phase shifts in the simulation are also within 12° . Both experimental and simulation found higher relative phase shifts around $y = 0$ mm at the smaller r_0 value. For the large absolute values of y , the relative phase shifts decreased for all cases. The angle a between the line of electric field and polarization vector of the laser increased when the y value increased. For larger a , the difference between the refractive indices in Eq. (29) decreased, as shown in Fig. 11. With the shorter distance r_0 , the relative phase shift decreased faster than with the longer r_0 . At around $y = -2$ mm in Fig. 10, the three lines representing the relative phase shifts for the three cases cross. This result is very similar to the one obtained by the experiment in Fig. 8. This result can be understood from the fact that the angle a is larger for the shorter distance r_0 at the same position of y as shown in Fig. 4.

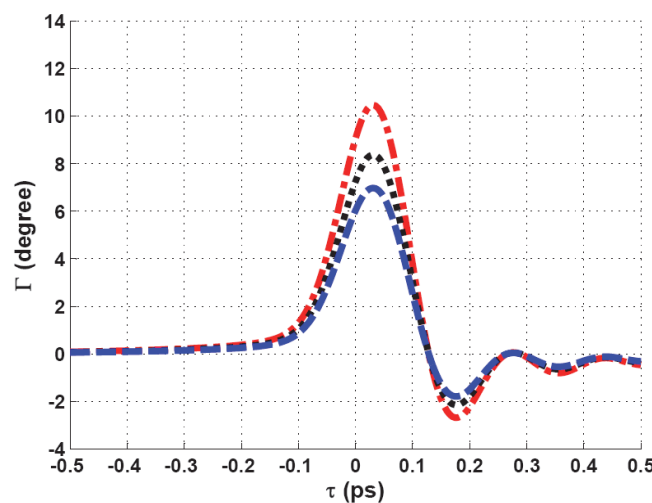


Fig. 9. Simulation result for the different distance r_0 at $y = 0$ mm ($a = 0^\circ$) case. The dash-dotted line is for $r_0 = 2$ mm, the dotted line for $r_0 = 2.5$ mm, and the dashed line for $r_0 = 3$ mm. τ is the delay time of the electron beam with respect to the laser arrival time to sample the electric field from the electron beam in the simulation. The beam charge q for the bunched part in the electron beam for the simulation is 0.1 nC.

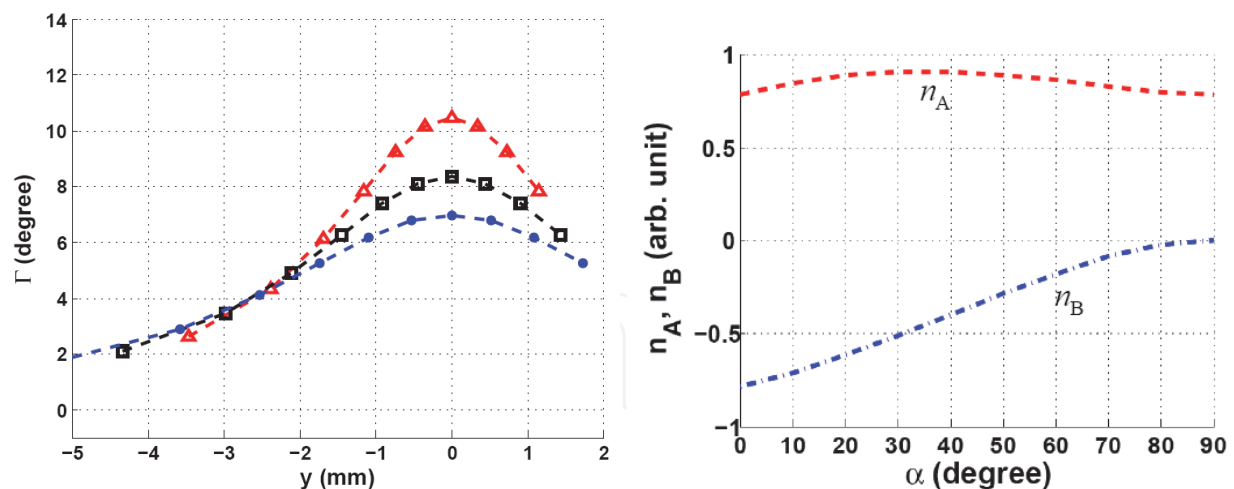


Fig. 10. Maximum relative phase shifts in Fig. 8 for different distances r_o with respect to the y are presented. The dots are the result with $r_o = 2$ mm, the squares with $r_o = 2.5$ mm, and the triangles with $r_o = 3$ mm. y is the laser passing position in the crystal along the angle α in Fig. 3. The beam charge q for the bunched part in the electron beam for the simulation is 0.1 nC.

Fig. 11. The refractive indices in Eq. (27) vs α .

6. Conclusion and discussion

We have derived refractive indices with the 45° decomposition axes with respect to the laser polarization vector in the plane perpendicular to the laser propagation direction with 3D configuration to decompose the laser polarization vector. We have also developed a theory for the detection of the optical power modulation. The experimental results are analyzed by the newly derived refractive indices. It is revealed that the laser is elliptically polarized from the fact that the relative phase shift is 12° at maximum.

We have also developed the simulation to understand experimental results correctly. The simulation shows that the maximum phase shift is about 12° , which is well agreed with the experimental result. The decreasing behavior of the relative phase shift in terms of larger $|y|$ is observed in the simulation result. While the relative phase shift for three different r_o cases is decreasing with different ratio, the phase shifts near $y = -2$ mm are crossed for three r_o cases. This also agrees well with the experimental result.

With the refractive indices derived in this study, we can open the way to express the polarization state of the laser in the electron beam measurement with EO crystal with a single quantity, i.e. the relative phase shift in Eq. (29). The relative phase shift shows a dependency on the incident angle of the laser to the EO crystal. To analyze the experimental result precisely, the newly derived refractive indices in this study will be a good tool in the diagnostics of the electron beam with EO crystal. We believe that the refractive indices in Eq. (29) must also be used in the analysis of the THz measurement result shown in Ref. [Shan et al., 2000].

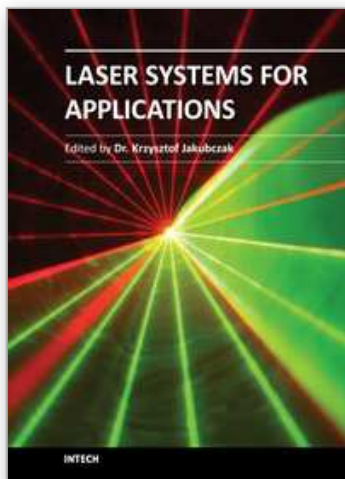
7. Acknowledgements

This work was supported by the Korea Science and Engineering Foundation (KOSEF) grant funded by the Korea government (Ministry of Education Science and Technology) (grant

No. 2008-0059842). One of authors (Y. W. Parc) extends his thanks to *Deutsches Elektronen Synchrotron (DESY)* for the hospitality during his stay (2006. Nov. ~ 2007. Apr.). Specially, we want to give great thanks to A. Azima for many discussions and for experimental help.

8. References

- [Azima et al., 2006] A. Azima, S. Dusterer, M. Huning, E. -A. Knabbe, M. Roehrs, V. Rybnikov, H. Schlarb, B. Schmidt, B. Steffen, P. Schmuser, A. Winter, M. Ross, Proceedings of European Particle Accelerator Conference 2006, Edinburg, Scotland, 1049 (2006).
- [Berden et al., 2004] G. Berden, S. P. Jamison, A. M. MacLeod, W. A. Gillespie, B. Redlich, A. F. G. van der Meer, *Phys. Rev. Lett.*, 93, 114802 (2004).
- [Casalbuoni et al., 2008] S. Casalbuoni, H. Schlarb, B. Schmidt, P. Schmuser, B. Steffen, A. Winter, *Phy. Rev. ST Accel. Beams*, 11, 072802 (2008).
- [Cavalieri et al., 2005] A. L. Cavalieri, D. M. Fritz, S. H. Lee, J. B. Hastings, et al., *Phys. Rev. Lett.*, 94, 114801 (2005).
- [Hecht, 2002] E. Hecht: *Optics* (Addison-Wesley, New York 2002) 4th ed., p. 336.
- [Jones, 1941] R. C. Jones, *J. Opt. Soc. Am.* 31, 488 (1941).
- [Par et al., 2007] Y. W. Parc, J. H. Park, C. B. Kim, J. Y. Huang, T. H. Joo, and I. S. Ko, *J. Korean Phys. Soc.*, 50, 1390 (2007).
- [Parc et al., 2008a] Y. W. Parc, C. B. Kim, J. Y. Huang, and I. S. Ko, *Nucl. Insrt. And Meth. A*, 586, 452 (2008).
- [Parc et al., 2008b] Y. W. Parc, J. H. Hong, C. B. Kim, J. Y. Huang, S. H. Lee, and I. S. Ko, *Jap. J. Appl. Phys.*, 47, 342 (2008).
- [Parc et al., 2009a] Y. W. Parc, I. S. Ko, *J. Appl. Opt. A: Pure Appl. Opt.*, 11, 105704 (2009).
- [Parc et al., 2009b] Y. W. Parc, I. S. Ko, *J. Korean Phys. Soc.*, 54, 1481 (2009).
- [Planken et al., 2001] P. C. M. Planken, H. K. Nienhuys, H. J. Bakker, and T. Wenckebach, *J. Opt. Soc. Am. B*, 18, 313 (2001).
- [Shan et al., 2000] J. Shan, A. S. Weling, E. Knoesel, L. Bartels, M. Bonn, A. Nahata, G. A. Reider, T. F. Heinz, *Opt. Lett.* 25, 426 (2000).
- [Shen et al., 2008] Y. Shen, G. L. Carr, J. B. Murphy, T. Y. Tsang, X. Wang, and X. Yang, *Phys. Rev. A*, 78, 043813 (2008).
- [Steffen et al., 2009] B. Steffen, V. Arsov, G. Berden, W. A. Gillespie, S. P. Jamison, A. M. MacLeod, A. F. G. van der Meer, P. J. Phillips, H. Schlarb, B. Schmidt, and P. Schmuser, *Phy. Rev. ST Accel. Beams*, 12, 032802 (2009).
- [Wen & Lindenberg, 2009] H. Wen and A. M. Lindenberg, *Phys. Rev. Lett.*, 103, 023902 (2009).
- [Wilke et al., 2002] I. Wilke, A. M. MacLeod, W. A. Gillespie, G. Berden, G. M. H. Knippels, A. F. G. van der Meer, *Phys. Rev. Lett.*, 88, 124801 (2002).
- [Yan et al., 2000] X. Yan, A. M. MacLeod, W. A. Gillespie, *Phys. Rev. Lett.*, 85, 3404 (2000).
- [Yariv & Yeh, 2003] A. Yariv and P. Yeh, *Optical Waves in Crystals: propagation and Control of Laser Radiation* (Wiley, New York, 2003), p. 229.



Laser Systems for Applications

Edited by Dr Krzysztof Jakubczak

ISBN 978-953-307-429-0

Hard cover, 308 pages

Publisher InTech

Published online 14, December, 2011

Published in print edition December, 2011

This book addresses topics related to various laser systems intended for the applications in science and various industries. Some of them are very recent achievements in laser physics (e.g. laser pulse cleaning), while others face their renaissance in industrial applications (e.g. CO₂ lasers). This book has been divided into four different sections: (1) Laser and terahertz sources, (2) Laser beam manipulation, (3) Intense pulse propagation phenomena, and (4) Metrology. The book addresses such topics like: Q-switching, mode-locking, various laser systems, terahertz source driven by lasers, micro-lasers, fiber lasers, pulse and beam shaping techniques, pulse contrast metrology, and improvement techniques. This book is a great starting point for newcomers to laser physics.

How to reference

In order to correctly reference this scholarly work, feel free to copy and paste the following:

Yong Woon Parc and In Soo Ko (2011). Quantification of Laser Polarization by Position Dependent Refractive Indices, Laser Systems for Applications, Dr Krzysztof Jakubczak (Ed.), ISBN: 978-953-307-429-0, InTech, Available from: <http://www.intechopen.com/books/laser-systems-for-applications/quantification-of-laser-polarization-by-position-dependent-refractive-indices>

INTECH
open science | open minds

InTech Europe

University Campus STeP Ri
Slavka Krautzeka 83/A
51000 Rijeka, Croatia
Phone: +385 (51) 770 447
Fax: +385 (51) 686 166
www.intechopen.com

InTech China

Unit 405, Office Block, Hotel Equatorial Shanghai
No.65, Yan An Road (West), Shanghai, 200040, China
中国上海市延安西路65号上海国际贵都大饭店办公楼405单元
Phone: +86-21-62489820
Fax: +86-21-62489821

© 2011 The Author(s). Licensee IntechOpen. This is an open access article distributed under the terms of the [Creative Commons Attribution 3.0 License](#), which permits unrestricted use, distribution, and reproduction in any medium, provided the original work is properly cited.

IntechOpen

IntechOpen